Measurement of the Power Spectral Density of the Fuel Spray in an Acoustically-Active Combustor

Chad M. Sipperley, Christopher F. Edwards

Department of Mechanical Engineering
Stanford University
Stanford, CA 94040, USA

Combustion instabilities in gas turbine and rocket combustors can cause catastrophic failures and is a limiting factor in improving the power densities of these devices. Research into the coupling between vaporization and combustion processes to the acoustic waves in the combustor is limited by a lack of a fundamental framework with which to measure the temporal behavior of the fuel spray. In this work we demonstrate the capability to measure the frequency content (power spectral density) of spray flows from analysis of phase-Doppler interferometry data. The technique is not limited to phase-synchronous data collection or to periodic or near-periodic spray flows.

We demonstrate this technique on a periodic spray flow with phase-locked data collection in order to evaluate the performance on a system of known frequency content. We demonstrate the ability to capture spectral resolutions with excellent accuracy (FWHM of 0.12 Hz about a 40 Hz fundamental, peak resolution to within 0.06 Hz across the bandwidth), good signal to noise (five orders of magnitude from the noise floor to the fundamental power spectral density), and wide bandwidth (DC to 7.5 kHz, with over 125 harmonics of the fundamental discernable).

After demonstrating the capabilities of this technique on a periodic system, we measure the power spectral density of a fuel spray in an acoustically-active can combustor. This system is not periodic, nor is there any phase information in the phase-Doppler data. We find that the spray flow contains power at the same frequencies as was measured in the thermoacoustic waves. We are also able to theorize a coupling mechanism between the thermoacoustic waves and the atomization/vaporization process from these data.

1. Introduction

Sprays are used in a number of applications where the temporal structure of the flow field is important. A prominent example is in the area of gas turbine combustion where it has been hypothesized that coupling between the vaporization rate of the drops and acoustic waves may contribute to thermoacoustic instability [1]. Another example is in the case of liquid rocket motors where compliance of the atomizer flow to pressure fluctuations can lead to severe oscillations [2].

In order to diagnose the role the spray plays in such systems, it is necessary to be able to measure the temporal structure—including the spectral content—of a spray. This is a non-trivial task in that a spray is composed of a number of discrete elements (the droplets) while

methods for spectral analysis have been developed assuming that a continuous signal (or a sampling of a continuous signal) is available.

In order to quantify the temporal dynamics of a spray it is necessary to develop a theoretical model within which to classify the spray. Edwards and Marx [3,4] developed such a system based upon the assumption that drop occurrence in sprays can be represented as a superposition of Poisson point processes. Investigation of inter-particle time analysis (time intervals between drop occurrences) [5,6] led to a technique to measure the power spectra of sprays. They demonstrated this technique on computer-generated, synthetic data generated *assuming* Poisson occurrence statistics.

In this work we demonstrate the technique on a spray of known (determinable) spectra: a phase-locked series of injections from a pulsed fuel injector. The periodic nature of the spray and phase-locked data acquisition allows a direct measure of the deterministic part of the spray's intensity function, and from this the power spectral density of drop occurrences can be found by Fourier transform. We then apply the technique to a spray flow for which no phase-lock information is available—the fuel spray of an acoustically active combustor. We compare the power spectral density of the spray to that of the pressure field inside the combustor.

2. Validation data set: Pulsed fuel injector spray

The validation experiment presented here is a gasoline direct injection fuel injector operated at 40 Hz. The "hold" voltage applied to the injector coil is 2 ms resulting in a duty cycle of 8%. The phase-Doppler interferometry (PDI) probe volume was placed along the outside edge of the fuel spray within 3 cm of the orifice (the white dot in Fig. 1). Rejection rates due to sizing, shape, and intensity errors were high. However, the parameter of interest is the arrival time of each drop so all arrival times were validated–only multiple droplets in the probe region at the same time were rejected.

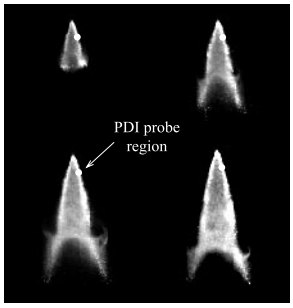

Fig. 1 Laser-sheet, Mie scattering images of the GDI pulsed injector at four different times after firing.

Though it might be appropriate to distinguish among various size/velocity classes in examining the dynamics of a spray, no such separation has been performed here. In this case, the entire spray is treated as a single class with no weighting by size or velocity. Also, PDI-related probe volume corrections must be applied to make accurate measures of spray intensities. Since we are comparing the same data with two different techniques, the lack of such corrections will have no impact on the evaluation of inter-particle time analysis–only on the true measure of the system dynamics.

Figure 2 plots the arrival times during three injector firings. The cycle frequency is quite evident in the clustering of the arrival times. Previous work [2] with computer-generated data

showed that large data sets would be required to calculate statistics of the spray intensity with precision. Therefore, 100 runs of 40,000 droplet arrivals spanning more than 61,000 injector firings were collected. To collect ensemble-averaged statistics there is no requirement that the sample time be long relative to the cycle time. However, in anticipation of the needs of inter-particle time analysis, this criterion has been met. The PDI probe volume used to measure the arrivals was very small to reduce the rejections due to multiple drops in the probe region at the same time–accounting for the low number of drops per pulse.

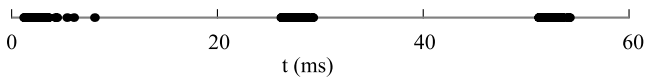

Fig. 2 Arrival timeline of a portion of the pulsed injector data; t_{cyc} = 25 ms. Each droplet arrival is represented by a circle. The apparent long bars are multiple, overlapping circles.

It is assumed that each injector firing is independent of the others. Therefore, every 25 ms of data represent an independent experiment or member of the ensemble. A histogram of arrival times is generated for each firing. The spacing chosen here provides 1024 bins per run (Δt = 24.4 μs). Given that there are, on average, only 65 arrivals per firing, most bins of the histogram will remain empty. The ensemble averaged spray intensity is generated from a summation of these bins for each run.

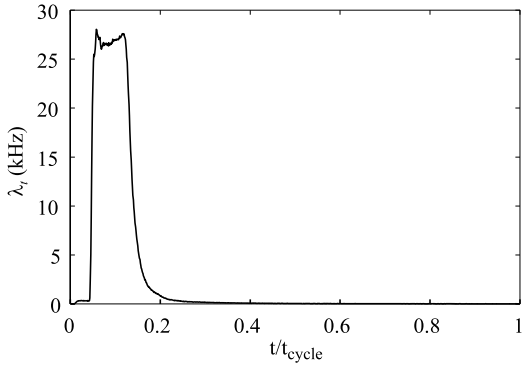

Fig. 3 Ensemble-averaged spray intensity vs. phase for the pulsed fuel injector.

Figure 3 plots the spray intensity (expected arrival rate) vs. phase for the pulsed injector. As expected from visual examination of the arrival timelines there is a large peak in the expected arrival rate during the firing of the injector. With such knowledge of the spray intensity, any statistics of interest are directly calculable.

Recall that the spray intensity is not a physical parameter that can generally be measured in a spray. It can only be measured by ensemble-averaging periodic systems with phase-synchronized data collection. We now apply the inter-particle arrival methodology to calculate the power spectrum of the spray intensity. This is done without relying on the phase information inherent to the data or on any assumptions of periodicity.

Figure 4 plots the all-gap inter-particle distribution function, $H_2(\tau)$, along with the autocorrelation of the ensemble-averaged spray intensity, $R_{\lambda\lambda}$. The first 50 ms of the all-gap function are plotted in Fig. 4. Unlike the autocorrelation of a periodic function, the all-gap function is defined for times longer than the cycle time. Not visible in the plot is a small

variation between the two correlation functions at near-zero time differences. This is an example of non-Poisson behavior of PDI data and is the focus of other research [7].

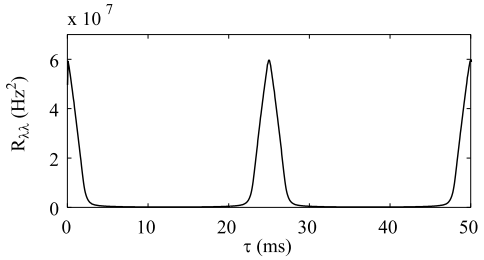

Fig. 4 Autocorrelation of the deterministic intensity function (Fig. 3) overlaps the autocorrelation determined from the all-gap interparticle time distribution.

We can now present the goal of this work: the power spectral density of the spray intensity function. Figure 5 is the discrete Fourier transform (DFT) of the autocorrelation of the spray intensity generated from the all-gap function. This is functionally equivalent to the right half of the (symmetric) two-sided power spectral density (PSD) of the spray intensity to within the resolution of the transform. Figures 5(a), (b), and (c) show the power spectrum over different frequency ranges. Plotted with the DFT of the all-gap function is the right half of the two-sided power spectrum (Fourier coefficients squared) of the ensemble-averaged spray intensity for qualitative comparison.

Since we are investigating a periodic system we expect sharp peaks in the power spectral density at the principle frequency and higher harmonics—the discrete representation of a series of delta functions. The principle frequency peak rises above the numerical noise floor by a factor of more than 10^5. Peaks associated with higher harmonics are discernable spanning five orders of magnitude of dynamic range through a frequency range of greater than 5 kHz—that is, beyond the 125^{th} harmonic of the principle frequency.

There are three noticeable features of the power spectral density to be highlighted. First, there is clearly a numerical "noise floor" at a power density of approximately 10^2 Hz^2Hz^{-1}. The value of this floor is determined by the size of the ensemble of the data collection. Longer data records result in a lower noise floor and a higher signal-to-noise ratio for features of interest.

Second, there is a deviation above 2.5 kHz between the values of the peaks of the power spectral density (PSD) and the power spectrum of the ensemble-averaged spray intensity. This is not necessarily a breakdown of the analysis technique. Ensemble averaging can only measure frequency content phase-locked to the data collection (i.e., the deterministic part of the spectrum). Any other uncorrelated signal (i.e., the stochastic part of the spectrum) will average to zero and will not contribute to the ensemble. Shot-to-shot variations in the injector pulses are one potential source of this high-frequency power. Another is shot-to-shot variations in the turbulent gas motion induced by the injection. Inter-particle time analysis, however, captures both the phase-locked (deterministic) and non-phase-locked (stochastic) power. As such, the power associated with any frequency interval as determined by inter-particle time analysis should be at least as large, if not larger, than that measured through direct transformation of the ensemble-averaged spray intensity function.

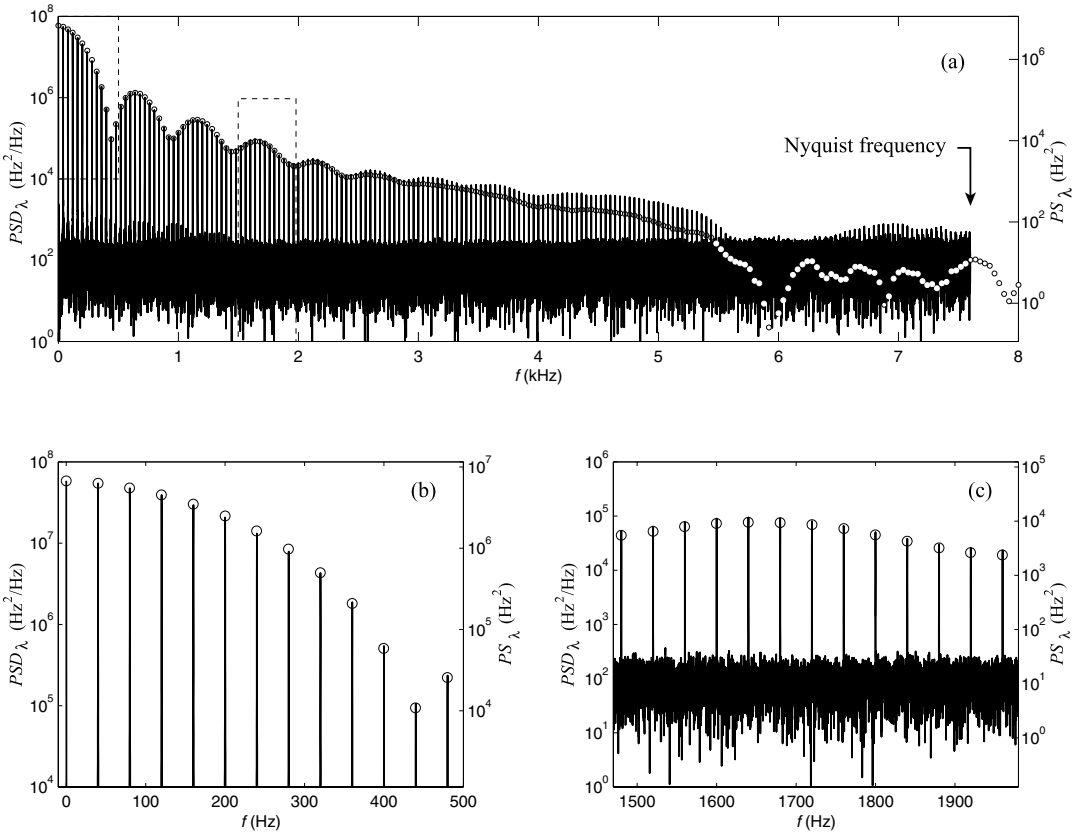

Fig. 5 Discrete Fourier transform of the all-gap distribution function, $H_2(\tau)$ (solid lines, left axis labels), as compared to the power spectrum of the ensemble-averaged spray intensity, λ from Fig. 3 (dashed lines and circles, right axis labels). Note that the inter-particle time analysis captures the principle and harmonic frequencies accurately.

Finally, there are peaks in the PSD at frequencies lower than 1.5 kHz that are not harmonics of the principle frequency. These peaks are a consequence of the finite bit depth inherent in the timing, exporting, and manipulation of drop occurrence times. Such finite bit depth introduces an artificial discretization to the possible time delays between drop arrivals. Finer resolution results in smaller spurious peaks. The data presented here were processed with double-precision mathematics. We note that if the data were manipulated in single-precision, the spurious peaks are two orders of magnitude larger in amplitude.

There are three ways to asses the quality of the power spectral density presented. The first is the location of the peaks. The principle frequency is at the system frequency of 40 Hz to within the resolution of the discrete transformation ($\Delta\nu$ = 0.06 Hz). In fact, all of the higher harmonics are centered at their respective frequencies to within 0.06 Hz—up to the Nyquist frequency of 7.6 kHz.

The second metric is a measure of true spectral resolution, including peak broadening due to numerical processing. The FWHM value of the 40 Hz peak is only 0.12 Hz—approximately twice the resolution of the DFT. To achieve these narrow peaks (and the high signal-to-noise

levels shown) it is necessary to window the all-gap function before performing the fast-Fourier transform. For this data we have used a Hanning (cosine) window function.

Table 1. Comparison of power measured by the indirect inter-particle time method with that obtained by a direct Fourier transform of the intensity function for the pulsed spray injector.

	Indirect Method	Direct Method	
f (Hz)	PSD Peak Area (Hz^2)	PS Fourier Coefficient^2 (Hz^2)	error (%)
40	6.44E+06	6.31E+06	2.13
80	5.76E+06	5.51E+06	4.42
120	4.84E+06	4.53E+06	6.89
160	3.81E+06	3.48E+06	9.38
200	2.78E+06	2.49E+06	11.67
240	1.86E+06	1.64E+06	13.59
280	1.12E+06	9.72E+05	14.98
320	5.82E+05	5.02E+05	15.93
360	2.45E+05	2.09E+05	17.18
400	7.11E+04	5.86E+04	22.48
440	1.67E+04	1.08E+04	54.28

A quantitative comparison between the DFT and the discrete power spectrum can be made by comparing the integrated power in the frequency interval represented by each Fourier coefficient. Table I gives the integral power of each peak for the principle frequency and first ten harmonics (integrated across 40 Hz bins centered on each frequency). Given the narrowness of the peaks, we speculate that the 2% error shown for the 40 Hz peak may be due to quadrature error in the integration. The 50% error shown for the 440 Hz peak seems large on first inspection, but one must realize that an error of ~6,000 Hz^2 is very small compared to the power of the full spectrum (3.5×10^7 Hz^2). Also, it is important to note that the total power as measured from the integration of the DFT in Fig. 5 across all frequencies is 10% higher than that from the sum of the power spectrum of the ensemble-averaged intensity. This is consistent with the presence of some frequency content that is not phase-locked to the injection. Note that a 10% level of excess power is equivalent to a 4.8% RMS stochastic fluctuation of the intensity about its deterministic component.

3. Fuel spray of an acoustically-active combustor

The true value of inter-particle time analysis is the ability to measure the frequency content of any arbitrary spray without need for synchronous data collection. Therefore, we have applied this analysis technique to phase-Doppler interferometry data collected from the fuel spray of an acoustically-active can combustor. Because this system is not a purely periodic system there is no phase information inherent in the data.

The combustor under study is a lean ($\phi = 0.5$), atmospheric-pressure, 80 kW hexane-air can combustor with two counter-swirled inlet air streams. The fuel nozzle is a pressure-swirl atomizer. The dominant acoustic mode is a half-wave mode at approximately 607 Hz between the inlet and outlet face plates. The RMS pressure fluctuation is 4 mbar at the acoustically-active operating point. Data was also collected at a non-acoustically-active

operating point just lean of $\phi = 0.5$ at a point where the RMS pressure fluctuations were reduced to 40 μbar. Phase-Doppler measurements were taken at multiple radial locations at a position of 50 mm downstream of the injector orifice.

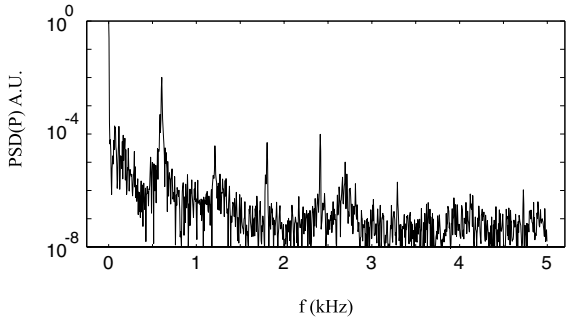

Fig. 6 Power spectra of the thermoacoustic instability of the pressure field.

Figure 6 is the discrete Fourier transform, power spectral density of the pressure transducer measurements of the combustor at the acoustically active operating point. The low frequency structure (below 100 Hz) is believed to be a quarter-wave mode in the air delivery section between the sonic choke and the combustor inlet (approximately 1 m long). The strongest peak is the half-wave mode at approximately 607 Hz. Harmonics of this frequency are seen at 1.2 kHz, 1.8 kHz, etc.

The goal of this research was to determine if there was any measurable coupling between the thermoacoustic waves and the spray statistics. Figure 7 demonstrates that, indeed, such coupling does appear in the PDI data. Figure 7 plots the power spectral densities of the fuel spray as measured by inter-particle time analysis. Data from multiple radial locations exhibited similar structure and, as such, only data from the maximum flux region of the fuel spray is shown here.

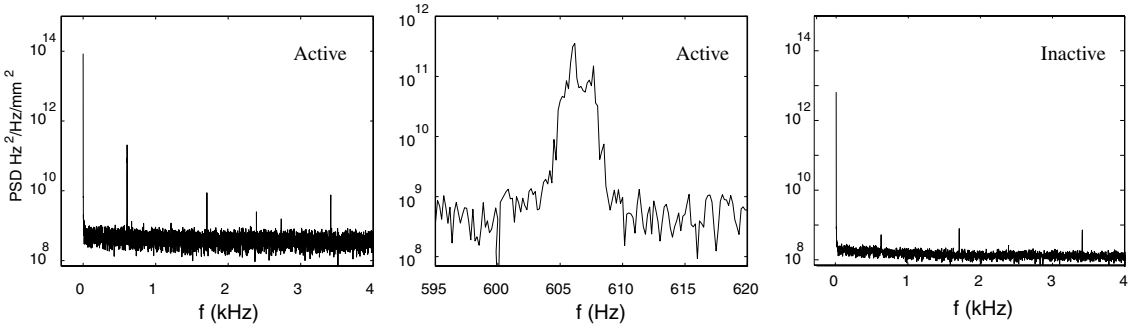

Fig. 7 Power spectra of the fuel spray intensity for two conditions. The left plot is a measure of the power spectra at the peak flux region of the fuel spray at the acoustically active operating point. The center figure is the same plot as the left with different axis limits chosen to focus on the first frequency peak. The right figure is the power spectra of the fuel spray at the acoustically-inactive operating point.

The strongest portion of the power spectra is at DC for both the acoustically-active and inactive cases. Only a small fraction of the spray intensity fluctuates at the dominant frequency. For the acoustically-active case, the integral power at the 607 Hz peak is

approximately 2% of the total power integrated from zero to the Nyquist frequency. For the acoustically-inactive case this number is 0.01%.

The width of the 607 Hz peak is much broader than the spectral resolution of the data set. This is in stark contrast to the pulsed injector data set. The difference, of course, is that the injector data set was generated from a stable signal generator whereas the combustor acoustics can support a band of frequencies around the half-wave mode with varying levels of attenuation.

When comparing the pressure PSD to the spectral content of the spray, it seems that the spray data shows sharper peaks than are seen in the pressure spectra. This may suggest that the coupling mechanism between the acoustics and the fuel spray in this combustor has its own frequency selection process. That is, there may be a non-linear response to the pressure field in such a way that drives the response to the peak power density of the pressure fluctuations.

As noted above, multiple data sets were taken at multiple radial locations across the fuel spray. All of these data exhibited similar characteristics in their spectra: all had strong peaks at 607 Hz and its harmonics. More so, the same characteristics could be seen in the power spectra of all the *size subclass* data at each location. One would expect that the smallest droplets in a fuel spray would react to the gas phase fluctuations. What came as a surprise was that even the largest droplets (> 60 μm) exhibited power at 607 Hz. This leads these researches to conclude that the origin of the spectral structure must occur at the source of the droplets, i.e. during atomization. We hypothesize that the pressure fluctuations within the combustor trigger instabilities in the intact sheet of the pressure-swirl atomizer near the orifice. These fluctuations then propagate downstream in the post-atomization environment.

4. Conclusions

We have demonstrated that inter-particle time analysis can be used to measure the frequency content of spray systems. A pulsed, periodic system was used to validate this technique and results were compared to statistics directly measured from the ensemble-averaged spray intensity. The power spectral density matched well both in frequency and magnitude accuracy. We went on to demonstrate that the fuel spray of an acoustically-active combustor may contain power at the same frequencies as the pressure fluctuations.

5. References

[1] A.Y. Tong, W A Sirignano 1987 ASME National Heat Transfer Conference.

[2] G P Sutton, O Biblarz 2001 Rocket Propulsion Elements (New York: John Wiley and Sons)

[3] C F Edwards, K D Marx 1995 Atomization and Sprays **5** 435-474

[4] C F Edwards, K D Marx 1995 Atomization and Sprays **5** 475-506

[5] C F Edwards, K D Marx 1996 Recent Advances in Spray Combustion **I** (ed. K K Kuo)

[6] K D Marx, C F Edwards 1994 The Sixth International Conference on Liquid Atomization and Spray Systems, ICLASS-94

[7] C M Sipperley, C F Edwards 2002 The Fifteenth Annual Conference on Liquid Atomization and Spray Systems, ILASS-Americas-02